Aleksander Lisiecki, Jan Orłowski, Santina Topolska

DOI: 10.327730/mswt.2024.68.3.2

Corrosion Resistance of Laser Beam Welded Joints in Ferritic Stainless Steel

Odporność korozyjna złączy spawanych laserowo ze stali nierdzewnej ferrytycznej

Abstract: The primary goal of the research work was to determine the corrosion resistance of laser beam-welded joints made of ferritic stainless steel X2CrTiNb18 (1.4509) having a thickness of 1.5 mm. In some of the test joints, the weld was subjected to rolling. In addition, some other joints were subjected to heat treatment involving the use of a prototype induction heating welding station. The research work-related test results revealed that the test joints with the weld subjected to rolling were characterised by a significantly lower rate of linear corrosion progression (linear corrosion rate V_p = 0.008672 mm/year) compared to the test joints only subjected to laser beam welding and those subjected to heat treatment (V_p = 0.011052 mm/ year).

Key words: laser beam welding, corrosion resistance, ferritic stainless steel, X2CrTiNb18

Streszczenie: Głównym celem badań było określenie odporności korozyjnej złączy blach ze stali nierdzewnej ferrytycznej X2CrTiNb18 (1.4509) o grubości 1,5 mm spawanych laserowo. Część złączy próbnych poddano operacji rozwalcowania spoiny, a część dodatkowo obróbce cieplnej na prototypowym stanowisku z nagrzewaniem indukcyjnym. Badania wykazały, że złącza próbne poddane operacji rozwalcowania spoiny wykazują wyraźnie niższą szybkość liniowego postępowania korozji (liniowa szybkość postępowania korozji V_p = 0,008672 mm/rok) w porównaniu ze złączami próbnymi spawanymi wyłącznie laserowo oraz z tymi poddanymi obróbce cieplnej (V_p = 0,011052 mm/rok).

Słowa kluczowe: spawanie laserowe, odporność korozyjna, stale nierdzewne ferrytyczne, X2CrTiNb18

1. Introduction

The laser beam welding of butt joints having a small thickness of up to 2.0 mm requires the very precise preparation of sheet edges with minimum deviations. The width of the gap between the front surfaces of sheets along the entire length of the joint cannot exceed 10 % of the sheet thickness, which, in the case of 1.5 mm thick sheets means that the gap width cannot exceed 0.15 mm [1, 2]. In addition, the high precision of the concentrated heat source (i.e. the laser beam having a focal diameter restricted within the range of 100 μm to 300 μm) requires high laser beam focus positioning accuracy in relation to the joint axis [34]. Moreover, when welding butt joints with butt welds, the range of optimum parameters is extremely narrow. Excessive linear welding energy leads to the incompletely filled groove ("weld face convexity") and, at the same time, excessive weld root convexity or even burn-through. In turn, overly low linear energy results in the lack of penetration (of sheets). However, the identification of welding parameters ensuring complete sheet penetration requires further parameter optimisation aimed at eliminating weld face and weld root undercuts as well as at ensuring the required height of excess weld metal [1-4].

Sheets, strips and sections made of chromium stainless steels usually have the ferritic microstructure (Feα) containing dispersive carbide precipitates ($(Fe,Cr)_{23}C_6$) and, in cases of stabilising agents (Nb and Ti), NbC and TiC carbides. Metallurgical products made of ferritic stainless steels are characterised by favourable formability and plasticity, whereas their cold work-triggered hardening (plastic strain) is smaller than that observed in austenitic steels [5, 6].

Ferritic stainless steels are considered to be characterised by relatively good weldability (in terms of metallurgical weldability). However, in order to ensure high joint properties, it is necessary to strictly follow related welding procedures and apply additional technological procedures. Most technological recommendations concerned with the welding of ferritic stainless steels apply to arc welding methods, e.g. welding with covered electrodes (or manual metal arc welding – MMAW), submerged arc welding (SAW) and gas-shielded welding (MIG/MAG and TIG). However, there are no detailed guidelines regarding the laser beam welding of the above-named group of steels. During laser beam welding, the mechanism of weld formation and the thermal effect on the material are different from those observed in relation to arc welding methods [5–7].

As a result, even the use of the most technologically advanced laser beam welding method does not eliminate all difficulties and problems connected with the welding of ferritic stainless steel grades [1, 4, and 8].

dr hab. inż. Aleksander Lisiecki, prof. PŚ, mgr inż. Jan Orłowski, dr hab. inż. Santina Topolska, prof. PŚ – Silesian University of Technology, Poland

Corresponding Author: aleksander.lisiecki@polsl.pl

The excellent properties of ferritic stainless steel can be lost as a result of the welding process (including laser beam welding). Welded joints are then characterised by reduced ductility, low toughness and susceptibility to corrosion. The reasons for such a situation include grain growth in the heat affected zone (HAZ) and the formation of martensite in the weld, favouring the susceptibility to cold cracking and joint brittleness, where susceptibility to corrosion often results from local chromium depletion in areas along grain boundaries [5, 6, 9].

For instance, in cases of accelerated cooling, particularly during laser beam welding, the weld and HAZ (in addition to ferrite) may contain some martensite, significantly reducing plasticity and potentially leading to the formation of cracks in the joint area [9].

Another issue is related to the grain growth in the single-phase structure. When heated to a temperature of more than 1350 °C, carbides undergo entire dissolution and the purely ferritic structure is formed, which, in turn, could lead to rapid grain growth. The coarse-grained structure is maintained (and irreversible) during cooling accompanying the $\delta \rightarrow \gamma$ transformation. For this reason, forged parts and sheets made of ferritic stainless steel are subjected to annealing at a temperature of 800 °C, aimed to ensure the obtainment of the ferritic structure with dispersive carbide precipitates [5, 6, and 10].

A serious problem accompanying the welding of ferritic stainless steels is connected with their high susceptibility to intercrystalline corrosion triggered by the thermal cycle and post-weld treatment conditions. The mechanism of intercrystalline corrosion is the same as that observed in chromium-nickel steel having an austenitic structure. The mechanism involves the precipitation of chromium-rich carbides and nitrides (usually in the area of grain boundaries), resulting from heating to high temperature and slow cooling restricted within the range of 400 °C to 600 °C. Carbides ($(Fe,Cr)_{23}C_6$ or $(Fe,Cr)_7C_3$) and nitrides (Cr_2N) precipitated under the above-named conditions are responsible for a decrease in the content of chromium. In addition, a decrease in the chromium content in the solution below 11 % leads to the loss of passivation. Such a state is referred to as sensitisation. In welded joints, the phenomenon of sensitisation affects primarily HAZ areas heated to temperatures triggering precipitation processes. In addition, the precipitation of carbides and nitrides in ferritic steels is faster and takes place at lower temperatures if compared to that observed in austenitic steels. One of the methods enabling the restriction of this unfavourable phenomenon involves the use of nitrogen and carbon-bonding additives such as Nb, Ti or Zr [5, 6, 7, 11, and 12].

Another issue encountered in relation to ferritic chromium steels and welded joints made of such steels is brittleness triggered by precipitation processes in the microstructure, particularly by the formation of intermetallic phases σ, and χ or Laves phases.

In cases of new-generation ferritic stainless steels, the improvement of weldability necessitated the reduction of carbon content to between 0.02 % and 0.08 % as well as the introduction of alloying agents of high chemical affinity for carbon and nitrogen (such as Ti, Nb and Al). Alloying agents stabilise the ferritic structure and bond all carbon and nitrogen contents into carbides and nitrides. Dispersive precipitates of NbC and TiC carbides inhibit grain growth at elevated temperatures, thus improving weldability [5, 6, and 13].

However, excessive contents of Nb and Ti additives and impurities (S, P) increase susceptibility to hot cracking triggered by the segregation of alloying components, impurities and the formation of low-melting eutectics along the grain boundaries.

Therefore, even in cases of the most advanced generations of the above-named ferritic steels, ensuring the optimal tensile strength and corrosion resistance of welded joints requires the precise selection of welding technological conditions and, frequently, the use of post-weld heat treatment.

In order to reduce internal stresses and temper martensite, the post-weld heat treatment of ferritic steels with low chromium content is performed within the temperature range of 750 °C to 800 °C [5, 6].

2. Tests

The principal objective of the tests was to determine the corrosion resistance of laser beam-welded joints made in 1.5 mm thick ferritic stainless steel X2CrTiNb18 (1.4509)

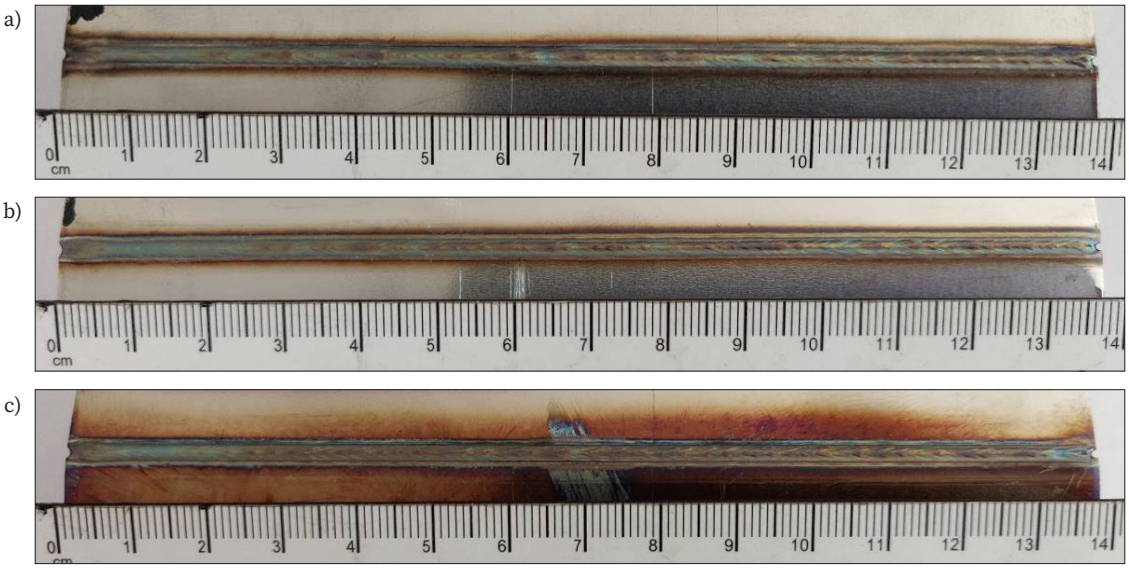

Fig. 1. Weld faces of selected test joints made in 1.5 mm thick steel X2CrTiNb18 (1.4509): a) laser beam-welded test joint, b) test joint after the rolling of the weld and c) test joint after the rolling of the weld, additionally subjected to heat treatment

sheets having dimensions of 100 mm ×140 mm. The test butt joints were made using a disc laser within parameters determined during previous tests (45 J/mm, 1.5 kW, 2.0 m/min) and meeting the quality-related criteria for the welding of catalytic converter and particulate filter housings. The test joints were welded without the use of shielding gas (the lack of the gas shielding of the weld face and root).

The welds of some of the test joints were subjected to rolling, whereas some others were subjected to heat treatment with induction heating performed using a power of 4.5 kW, a frequency of 10 kHz, a travel rate (in relation to the hairpin inductor) of 100 mm/min and a distance from the exciter of 15 mm. The corrosion tests involved a total of 10 specimens, including three specimens of each test joint type and one specimen of the base material, treated as a reference specimen (Fig. 1). The corrosion tests were performed in an artificial salt mist environment in a dedicated chamber, following the requirements of the PN-EN-ISO 9227 standard. In addition, the additional assessment of the quality of the test joints entailed the performance of visual tests (VT), macro- and microscopic observations of metallographic specimens and cross-sectional hardness measurements.

The preparation of specimens for the microscopic and corrosion tests was performed in the laboratories of the Faculty of Mechanical Engineering using the following machines, testing equipment and materials:

- disc cutting machine (Metkon SERVOCUT-M300),
- grinder (ATM SAPHIR 250 M2),
- microscope (Nikon ECLIPSE MA 100),
- chamber for cyclic corrosion tests (CCP450ip) (Fig. 2).

The specimens used in the metallographic tests were included in epoxy resin. Afterwards, the surfaces of the specimens were subjected to automatic grinding and polishing with an ATM SAPHIR 250 M2 machine using abrasive paper having a granularity of 400, 800, 1200 and 2500. The surfaces of the metallographic specimens were polished with ATM GALAXY OMEGA and SIGMA discs having a diameter of 250 mm and Metkon DIAPAT-M slurry having a granularity of 3.0 µm and 1.0 µm. The final stage of polishing was performed using silica slurry having a granularity of 0.5 µm. After each change of the abrasive paper, the specimen was turned by an angle of 90° (in order to ensure the uniform grinding of the surface). The specimen surfaces were cleaned with spirit having a concentration of 95% and dried with a compressed air jet. After polishing, the surfaces of the metallographic specimens were degreased and etched in the solution of nitrohydrochloric acid (the so-called aqua regia).

Fig. 2. Chamber (CCP450ip) used in cyclic corrosion tests in the laboratory of the Faculty of Mechanical Engineering of the Silesian University of Technology in Gliwice

The metallographic tests were performed using an ECLIPSE MA 100 and SZX9 optical microscopes (Nikon and Olympus respectively) as well as a NISELEMENT BR 3.2 software programme, supporting metallographic tests. The microstructure of selected test joints is presented in Fig. 3.

The corrosion tests involved the use of specimens sampled from the test joints immediately after welding (WJ), after the rolling of the weld (RW) after additional heat treatment (HT) and from the base material of steel X2CrTiNb18 sheets (BM) (reference specimen). The edges and cut surfaces were protected with varnish to slow down the progression of corrosion in these areas. The corrosion tests in the salt spray chamber (Ascott) were performed in accordance with PN-EN ISO 9227 standard, using the NSS method (neutral salt spray) and standard parameters of the aforesaid method.

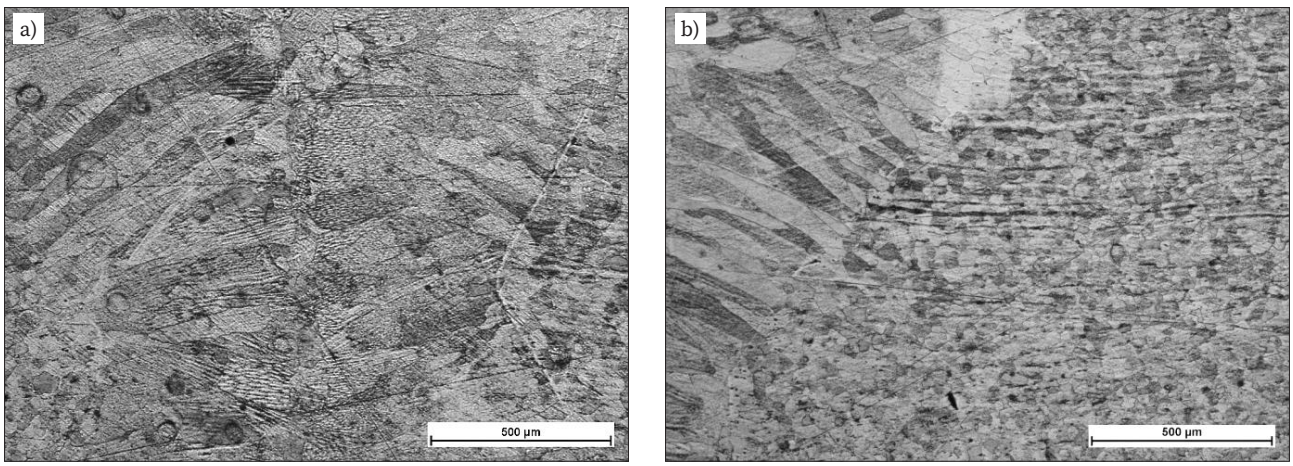

Fig. 3. Microstructure of the test joint area (from the left: weld/fusion line/HAZ): a) joint after the rolling of the weld and b) joint subjected to heat treatment

The assessment of the corrosion progression degree under artificial salt spray conditions involved the use of two methods, i.e. qualitative visual assessment by the unaided eye, aimed at identifying areas where corrosion progression was the most intense and gravimetric method-based quantitative measurements, consisting in assessing changes in the mass of the specimen in relation to the active area of a given specimen (in accordance with the PN-H-04608 standard). Before the tests performed in the salt spray chamber, the mass of the specimens as well as the width and the length of the joint were measured (in order to calculate the active area of the specimen). The dimensions of the specimens are presented in Table 1.

In accordance with the related standard, subsequent mass measurements for gravimetric calculations and photographs of the specimen surfaces for visual assessment

Table 1. Dimensions and the active area of the specimens subjected to the corrosion tests in the salt spray chamber

Specimen designation	Length [mm]	Width [mm]	Thickness [mm]	Specimen active area [m^2]
MR	151	103	1.5	0.015553
SP	151	101	1.5	0.015251
RS	154	104	1.5	0.016016
OC	154	101	1.5	0.015554

Table 2. Calculation results of specimen daily mass depletion in time

	Daily mass depletion $\left[\left(\frac{g}{m}\right)^2 24\ h\right]$		
Nr próbki	**24 h**	**96 h**	**186 h**
MR	0.085728	0.080906	0.087872
SP	0.271020	0.173759	0.237924
RS	0.197719	0.141525	0.209612
OC	0.250739	0.208414	0.240330

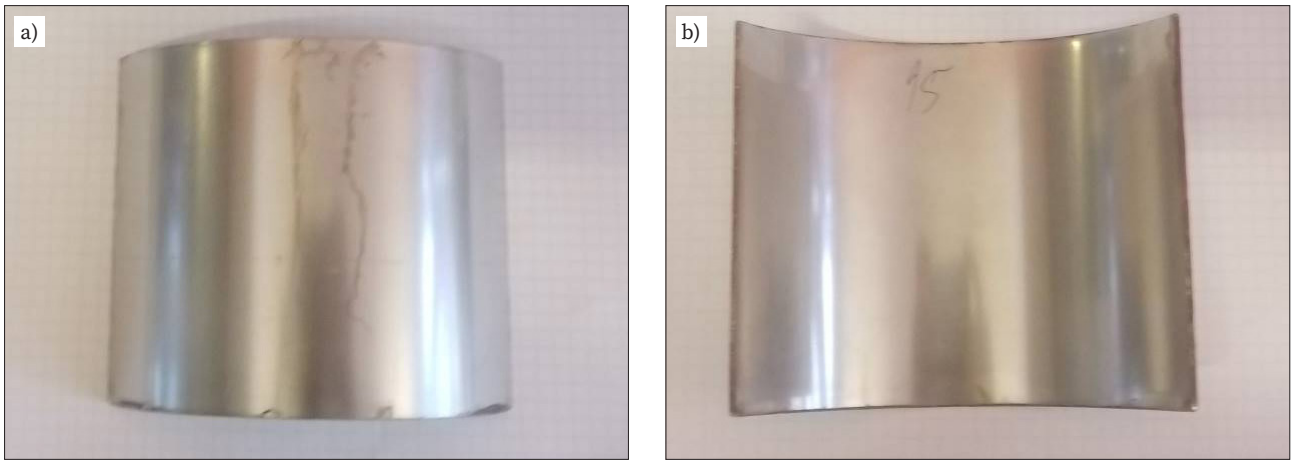

Fig. 4. Base material (BM) after 168 hours of the test in the salt spray chamber: a) external surface of the specimen (tube) and b) internal surface of the specimen

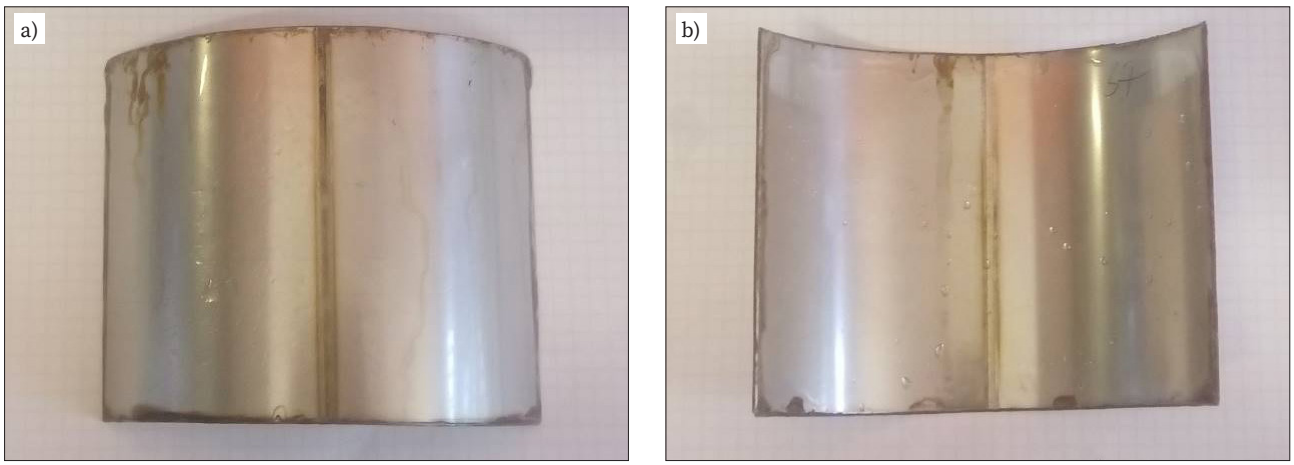

Fig. 5. Surface of the laser beam welded joint (LW) after 168 hours of the test in the salt spray chamber: a) weld face and b) weld root

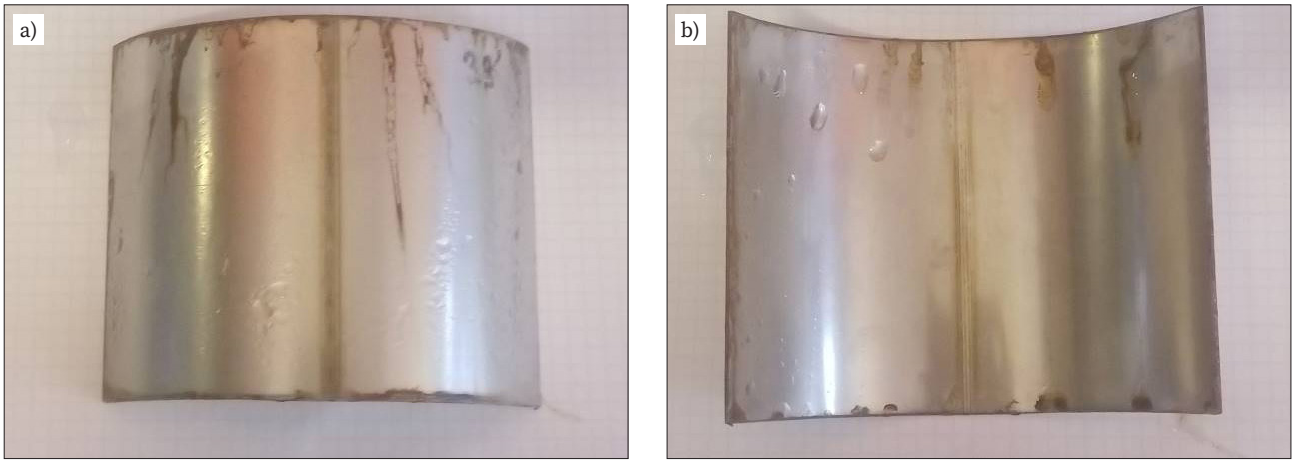

Fig. 6. Test joint with the rolled weld (RW) after 168 hours of the test in the salt spray chamber: a) weld face and b) weld root

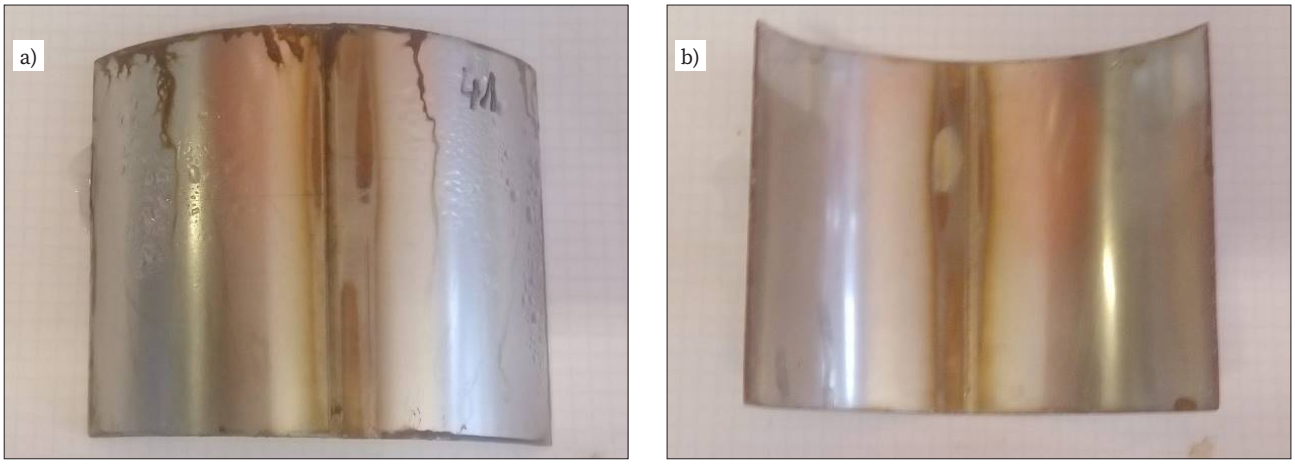

Fig. 7. Test joint with the rolled weld, subjected to heat treatment (HT), after 168 hours of the test in the salt spray chamber: a) weld face and b) weld root

were performed following the tests in the salt spray chamber lasting 24, 96 and 168 hours respectively. Comparative photographs for visual assessment were taken before the removal of corrosion products from the specimen. The specimen mass was measured using an AS 310/X analytical balance (RADWAG), having a full measurement range of 310 g and a measurement accuracy of 0.0001 g. The results of specimen mass measurements on subsequent days of the tests are presented in Table 2, whereas the specimens during the corrosion tests are presented in Figures 4–7.

3. Analysis of test results

The microscopic tests and observations revealed the clearly visible fusion line of the test joints, the narrow heat affected zone (HAZ) and slight grain growth in the HAZ area. The weld area contained characteristic columnar grains, oriented perpendicularly to the fusion line. The microstructure of the base material and that of the welds was characterised by the dominant content of ferrite.

The visual tests revealed the presence of a crater at the end of each test joint and the slightly incompletely filled groove (Fig. 1). The width of the weld face was uniform along the entire length and restricted within the range of 2.5 mm to 3.5 mm. The laser beam welded joint with the rolled weld was characterised by narrow discolouration along the axis (having a width of less than 1.5 mm on each side). In turn, in terms of the test joint subjected to additional heat treatment, it was possible to observe the clearly visible oxidation of the joint surface (having a width of approximately 10 mm to 15 mm on each side of the joint). The weld face surfaces were flat and even. In addition, the test joint surfaces did not contain porosity or cracks.

The visual tests (VT) also revealed that the mechanical cutting of the specimens (with a circular saw) led to the significant roughness of cut surfaces and edges, which, in turn, made it difficult to properly protect the above-named areas and isolate them from the corrosive environment. It was found during the corrosion tests performed in the artificial salt spray atmosphere that corrosion was initiated and progressed intensively in the specimen cut area. In terms of the base material (BM), corrosion products were only observed in the area of the specimen cut area and local corrosion centres triggered by the flow of corrosion products from the cut areas.

In turn, as regards the specimens of the joints (LW, RW, HT) subjected to corrosion tests, it was observed that the solution of salt led to the gradual removal of discolouration along the joints, which was particularly visible in the specimen subjected to heat treatment (HT), where the area of discolouration was relatively wide. In addition, in terms of the welded joint specimen not subjected to any other procedures (LW) and that subjected to heat treatment (HT), it was possible to observe local corrosion centres along the weld axis. The corrosion centres were located in the scratched areas of the sheet surfaces (local surface damage).

4. Gravimetric tests

The gravimetric analysis involved the assessment of the corrosion progression rate based on the measurements of changes in specimen mass in relation to the active cross-section of the specimen affected by the corrosive factor. For this reason, the analysis involved the determination of the area of each specimen (Table 1).

The unitary mass depletion rate observed in the specimens within 24 hours was determined using the following formula (1):

$$V_c = \frac{\Delta G}{At} \tag{1}$$

where:

V_c – mass depletion $\left[\frac{g}{m^2 \cdot 24\ h}\right]$,
ΔG – change in specimen mass [g],
A – active area of the specimen before corrosion [m^2],
t – corrosion duration [24-hour cycles].

In turn, the linear corrosion progression rate (changes in specimen cross-section) was determined using the following dependences (2, 3, Table 3):

$$V_p = V_c a \tag{2}$$

$$a = \frac{365}{1000d} \tag{3}$$

where:

V_p – linear corrosion progression rate [mm/year],
a – coefficient linking specimen mass depletion to the linear corrosion progression rate,
d – material density $\left[\frac{g}{cm^3}\right]$.

The results of the corrosion tests, those of the mass depletion measurements and calculated linear corrosion progression values enabled the identification of the corrosion resistance of the base material and the laser beam welded test joints (Table 4).

The corrosion tests and mass depletion measurements revealed that the highest corrosion resistance under test conditions was that of the base material of steel X2CrTiNb18 (BM). In terms of the base material, the mean linear corrosion progression rate amounted to 0.004021 mm/year, enabling the classification of the steel as resistant to corrosion and representing the 2nd degree of corrosion resistance (Table 4). In turn, the laser beam welded joint with the weld subjected to rolling (RW) was characterised by the mean linear corrosion progression rate amounting to 0.008672 mm/year, enabling the classification of the steel as very resistant to corrosion and representing the 3rd degree of corrosion resistance (Table 4). However, it should be noted that the above-presented results were close to the upper limit of the aforesaid degree of corrosion resistance.

The laser beam welded joint not subjected to additional technological treatments (LW) was characterised by a linear corrosion progression rate of 0.010787 mm/year, making the steel classified corrosion-resistant and representing the 4th degree of corrosion resistance (Table 4). The laser beam welded joint subjected to heat treatment (HT) with the rolled weld was characterised by a linear corrosion progression rate of 0.011052 mm/year, which enabled its classification among corrosion-resistant steel also in the 4th degree of corrosion resistance (Table 4). It should be noted that the corrosion resistance values of the laser beam welded joints (LW) and the laser beam welded joints subjected to heat treatment (HT) were close to the lower limit of the 4th degree of corrosion resistance.

Table 3. Linear corrosion progression rate values, V_p

	Linear corrosion progression rate [mm/year]			
Specimen no.	**24 h**	**96 h**	**186 h**	**średnia**
MR	0.004064	0.003835	0.004165	0.004021
SP	0.012847	0.008237	0.011278	0.010787
RS	0.009372	0.006709	0.009936	0.008672
OC	0.011886	0.009879	0.011392	0.011052

Table 4. Corrosion resistance (in accordance with PN-H-04608)

Group of corrosion resistance	Designation	Degree of corrosion resistancej	V_p [mm/rok]
Fully resistant	I	1	below 0.001
Very resistant	II	2	above 0.001 up to 0.005
		3	above 0.005 up to 0.01
Resistant	III	4	above 0.01 up to 0.05
		5	above 0.05 up to 0.1
Less resistant	IV	6	above 0.1 up to 0.5
		7	above 0.5 up to 1.0
Little resistant	V	8	above 1.0 up to 5.0
		9	above 1.0 up to 5.0
Not resistant	VI	10	above 5.0 up to 10.0
			above 10.0

5. Conclusions

The laser beam welded butt joints made of 1.5 mm thick ferritic stainless steel X2CrTiNb18 without using the filler metal were characterised by reduced corrosion resistance in comparison with that of the base material. However, because of the narrow width of the weld, even the welded joint specimens could be rated among very corrosion-resistant steels (3rd degree of corrosion resistance) or corrosion-resistant steels (4th degree of corrosion resistance). Among the test joint specimens, the highest corrosion resistance was observed in the joint specimens with the rolled weld (RW); these specimens could be classified as very corrosion-resistant steels (3rd degree of corrosion resistance).

Publication supported within the programme of Excellence Initiative – Research University (10/050/SDU/10-21-01) implemented at the Silesian University of Technology, the year 2022/24.

Article submitted to the 28th Scientific and Technical National Welding Conference "Progress, innovations and quality requirements of welding processes"(Międzyzdroje, 21-23.05.2024 r.)

REFERENCES

[1] Lisiecki A., Kurc-Lisiecka A., Pakieła W., Topolska S.: Microstructure and properties of Laser-welded butt joints of X2CrTiNb18 steel. International Journal of Modern Manufacturing Technologies (IJMMT). 2023, vol. 15, no. 1, pp. 25-33.
[2] Lisiecki A., Rokita Z., Ginalski D., Kośny A., Pakieła W.: Laser welding of ferritic stainless steel 1.4509 used in the manufacturing of catalyst housings and diesel particulate filters. Biuletyn Instytutu Spawalnictwa, 2022, vol. 66, no. 3, pp. 7-17.
[3] Kurc-Lisiecka A., Lisiecki A.: Laser welding of stainless steel. Journal of Achievements in Materials and Manufacturing Engineering. 2020, vol. 98, no. 1, pp. 32-40.
[4] Kotarski P., Lisiecki A., Żuk M.: Badanie technologii zautomatyzowanego doczołowego spawania laserowego blach ze stali nierdzewnej. Spajanie Materiałów Konstrukcyjnych. 2020, no. 1 (47), pp. 22-24.
[5] Łabanowski J.: Stale odporne na korozję i ich spawalność. Politechnika Gdańska, Gdańsk 2018, p. 190. ISBN 978-83-7348-756-7.
[6] Brytan Z.: Vademecum stali nierdzewnej. Stowarzyszenie Stal Nierdzewna, Warszawa 2018, p. 195. ISBN 978-83-940143-1-5.
[7] Świerczyńska A., Fydrych D., Landowski M., Rogalski G., Łabanowski J.: Hydrogen embrittlement of X2CrNiMoCuN25-6-3 super duplex stainless steel welded joints under cathodic protection. Construction and Building Materials. 2020, vol. 238, no. art. 117697. https://doi.org/10.1016/j.conbuildmat.2019.117697.
[8] Brytan Z., Pakieła W.: Laser Surface Treatment of Sintered Stainless Steels for Wear Resistance Enhancement. Key Engineering Materials. 2019, 813, pp. 221-227. https://doi.org/10.4028/www.scientific.net/kem.813.221.
[9] Rogalski G., Jurkowski M., Łabanowski J., Fydrych D.: Effect of the post-weld surface condition on the corrosion resistance of austenitic stainless steel AISI 304. Biuletyn Instytutu Spawalnictwa, 2018, vol. 62, no. 1, pp. 17-23.
[10] Brytan Z.: The corrosion resistance of laser surface alloyed stainless steels. Journal of Achievements in Materials and Manufacturing Engineering. 2018, vol. 91, no. 2, pp. 48-59.
[11] Świerczyńska A., Łabanowski J., Michalska J., Fydrych D.: Corrosion behavior of hydrogen charged super duplex stainless steel welded joints. Materials and Corrosion. 2017, vol. 68, no. 10, pp. 1037-1045.
[12] Lisiecki A., Kurc-Lisiecka A., Topolska S.: Corrosion resistance of laser welded sheets of stainless steel 316L. International Journal of Modern Manufacturing Technologies. 2022, vol. 14, no. 3, pp. 171-175. https://doi.org/10.54684/ijmmt.2022.14.3.171.
[13] Juroszek W., Kurc-Lisiecka A., Lisiecki A.: Odporność korozyjna złączy blach ze stali austenitycznej spawanych laserowo. Fastener, 2020, no. 3-4, pp. 12-20.